Chapter 2
New Hamiltonian Semi-analytical Approach for 3D Solution of Piezoelectric Smart Composites

Orlando Andrianarison and Ayech Benjeddou

Abstract This chapter addresses the development of a new semi-analytical Lagrangian-Hamiltonian method for the three-dimensional solution of piezoelectric smart composite plates. It is based on the analytic *state space symplectic Hamiltonian approach* to fulfil the electromechanical multilayer interface continuity constraints and two-dimensional *in-plane finite element* (FE) numerical discretization to deal with arbitrary boundary conditions (BC) on the composite lateral edges. The originality of the proposed semi-analytical solution is that the latter feature (arbitrary BC handling) is reached through a mechanical displacements-electric potential primary variables-based Lagrangian formalism, while the solution accuracy feature is reached through a primary and dual (transverse stresses and electric displacement) variables-based partial mixed Hamiltonian formalism. The transformation of the Lagrangian FE discretized formulation to a state space Hamiltonian one is made through the Legendre transformation. The proposed methodology is applied to the static actuation and sensing of *piezoelectric* hybrid laminated composite plates subjected to various BC. The obtained results comparison to reference ones of various benchmarks solutions, for non classical BC (cantilever), multilayer composite layups (angle-ply) and electromechanical loadings (uniform), from the open literature shows good computational convergence (coarse mesh), low cost (few FE degrees of freedom) and high accuracy (exact through-the-thickness) of the present new Hamiltonian semi-analytical solutions. Thus, the provided tabulated numerical results can be used safely for benchmarking other closed-form, numerical or semi-analytical solutions.

Orlando Andrianarison
Institut Supérieur de l'Automobile et des Transports, 49 rue Mademoiselle Bourgeois, 58000 Nevers, France
e-mail: orlando.andrianarison@u-bourgogne.fr

Ayech Benjeddou
Institut Supérieur de Mécanique de Paris, 3 rue Fernand Hainaut, 93400 Saint Ouen, France
& ROBERVAL, FRE 2012 UTC/CNRS, rue Personne de Roberval, 60200 Compiègne
e-mail: benjeddou@supmeca.fr, ayech.benjeddou@utc.fr

H. Altenbach et al. (eds.), *Analysis of Shells, Plates, and Beams*, Advanced Structured Materials 134,
https://doi.org/10.1007/978-3-030-47491-1_2

Key words: Lagrangian finite element · Partial-mixed state space · Symplectic Hamiltonian · Three-dimensional semi-analytic solution · Piezoelectric actuation and sensing · Multilayer composites

2.1 Introduction

Structural elements made of *composite* materials are already being used for a long time in various fields of engineering. The range of their applications covers several branches of industries such as aircraft and automotive constructions, medical equipment or marine and civil engineering. Nowadays, the research activities on composites mostly evolve to the integration (surface-bonding or embedding) of the so-called *smart* materials. Among the latter, the *piezoelectric* sensors and actuators are being widely used thanks to their undeniable advantages, like excellent electromechanical coupling properties, low cost fabrication, design flexibility and, most importantly, applicability in vibration control, health monitoring and damage prognosis of load-carrying structures.

Over the past few decades, considerable efforts have been devoted to the development of theories and numerical modelling of smart piezoelectric laminated composites and structures (Benjeddou, 2000; Kapuria et al, 2010; Li, 2020). It appears that the main issues are the computational cost and accuracy. Indeed, it is a fact that they are anisotropic and three-dimensional (3D) in nature. Thus, their accurate electromechanical modelling requires appropriate descriptions of their mechanical and electrical variables, particularly through the thickness direction. The compatibility and equilibrium conditions at the interfaces state that an efficient modelling of such structures must deal with the so-called *interface continuity* (IC) constraints; namely, the continuity of the transverse (out-of-plane) mechanical stresses and electric displacement through the interfaces of the laminate. Among the numerous models and tools available in the literature, only few can cope with these specific features; nevertheless, natural theoretical frameworks to deal with these requirements are the full/hybrid (Sze and Pan, 1999) and partial (Carrera et al, 2010) mixed ones.

Analytically, the mixed *state space method* (SSM) that uses the mechanical displacements and electric potential variables, augmented with the transverse stresses and electric displacement as independent variables (Benjeddou and Deü, 2001), is a good example of *partial-mixed* frameworks. However, it is limited by the a priori fulfilment of the boundary conditions (BC) and cross-ply laminate schemes so that it is not usable for realistic BC other than the full simply-supported (SS) ones. The practical cantilever (clamped-free) BC have been considered (Leung et al, 2008) analytically through the exact symplectic approach, which review (Lim and Xu, 2010) shows other solutions for various BC combinations with the classical SS ones. Alternative approaches to the purely analytical ones are the so-called semi-analytical solutions (Wu and Liu, 2016) which combine in-plane numerical discretization, such as the finite element (FE) method, and through-the-thickness analytical methods, such as the SSM. Only the authors' earlier work (Andrianarison and Benjeddou,

2012) was cited, in the previous review (Wu and Liu, 2016), in the category of state space-FE semi-analytical solutions for the quasi-3D analysis of smart composites and functionally graded materials. Another type of semi-analytical methods was also suggested in Benedetti et al (2010) for the 3D analysis of damaged structures, modelled by the numerical dual boundary element method, with bonded piezoelectric sensors, modelled by the analytical SSM.

Numerically, 3D full/hybrid (Sze and Pan, 1999) and mixed FE are suitable but expensive, due to the thinness of the multilayer plies that often requires fine meshes. Partial-mixed *variational formulations* (VF) that use the mechanical displacements and electric potential, augmented with the transverse stresses and transverse electric displacement through Lagrange multipliers, are a good alternative for reducing the number of independent variables (Benjeddou and Andrianarison, 2005). By retaining the primary variables along with their dual ones, the aforementioned mixed formulations share a common mathematical issue: they must be able to satisfy the so-called *Brezzi-Babuška* (BB) inf-sup conditions (Boffi et al, 2013). This saddle-point property of the mixed VF in general is of crucial importance in the effectiveness of such formulations. To tackle this issue, a *Layer-Wise* (LW) mixed least-square framework was presented in Moleiro et al (2015) for example. Another option that permits to deal with the special requirements of the smart laminated composites modelling is to use the *semi-analytical* approach that combines an analytical mixed SSM through-the-thickness and a numerical discretization of the reference plane. Its major advantages are the significant reduction of the computational cost and the increase of the solution accuracy. The starting point of the retained semi-analytical method consists in decomposing the 3D volume into a reference two-dimensional (2D) in-plane domain and a one-dimensional transverse direction, in combination with the application of the method of separation of variables. The high-order 3D partial differential equilibrium equations are then solved exactly along the transverse direction thanks to the SSM, whereas a weak solution is searched in the reference plane. Therefore, the main issue of semi-analytical methods concerns the chosen numerical method to discretize the 2D in-plane problem. For example, the method developed in Shan et al (2018) aims at applying the scaled boundary FE method to the static bending of a piezoelectric beam. In Zhou et al (2020), the traditional FE method is used to compute the deformation of general curved beams under various BC. A similar approach is presented in Zhou et al (2015) where a state space-FE semi-analytic approach is used to study the cylindrical bending of a straight cantilever beam. Under plane strain conditions of elasticity (cylindrical bending), the 3D governing equations transform into a two-point boundary value problem (BVP) so that a numerical method can be bypassed for the benefit of an analytic method such as the eigenfunction expansion. This is done in Zhang and Wang (2018) where the axisymmetric static deformation of a piezoelectric cylinder under arbitrary BC is investigated in the framework of a Hamiltonian symplectic superposition approach. Through the literature review in the ongoing section, the partial mixed VF, assorted with the semi-analytical approach, therefore constitutes a suitable framework for modeling piezoelectric smart composites. Indeed, this allows a straightforward fulfilment of the laminate transverse stresses and electric displace-

ment IC without cumbersome manipulations (Khandelwal et al, 2013) as for the equivalent single–layer or LW classical 2D models.

Alternatively to the classical Lagrange-type formulations, the partial mixed VF presented in Andrianarison and Benjeddou (2012) has been derived in the framework of the *Hamiltonian* formalism after a Legendre transformation. The latter allowed the natural introduction of the transverse stresses and electric displacement as primary variables, and maked the final partial differential equations (PDE) lower in order, compared to the Lagrange-type formulations. Besides, the Hamiltonian formalism allowed transforming, in a systematic way, the equations of 3D piezoelectricity (4th order PDE) into first-order linear ordinary differential equations (ODE) for which the coordinate in the thickness direction is the only independent geometric parameter. This feature appears to be interesting in the perspective of developing efficient numerical tools for multilayer smart composites since the propagator matrix approach, used for the analytical mixed SSM, can then be exploited. Thus, the resulting model simplifies considerably the computational treatment of the IC, leading potentially to accurate predictions of the detailed response characteristics, such as the through-the-thickness distributions of the state variables. However, recasting the classical VF into a mixed one has also some inevitable drawbacks. As a matter of fact, by incorporating the transverse stresses and electric displacement as dual variables into the VF, the question of the proper treatment of the BC arises for realistic ones other than SS. Indeed, the use of the SSM to compute the through-the-thickness distributions of the state variables implicitly requires that the final matrix is square so that its exponential function can be used. This requirement determines the well-posedness of this approach and explains why the VF in Andrianarison and Benjeddou (2012) is only efficient for the theoretical SS BC; indeed, it can be shown that the problem is well-posed if and only if the number of primal and dual variables to be constrained on a given edge is equal, as is the case for the well-known Navier-type analytical solutions.

In summary, according to the above discussion, it appears that the use of the partial mixed VF is relevant since it makes possible the fulfilment of the IC conditions when needed. However, the corresponding numerical models are non-standard and must be used with care due to the BB stability conditions. Moreover, the use of the Hamiltonian framework in combination with the partial Legendre transformation offers a good compromise between high needs of computer resources of LW approaches and complexities of the 3D full mixed VF. Therefore, the purpose of this chapter is to present a new partial-mixed VF where the above mentioned drawbacks are circumvented by choosing a new set of dual stress-like variables that coincide with the out-of-plane *nodal* transverse stresses-like *resultants*. This can be seen as one of the main original contributions of the present work. Moreover, a semi-analytic procedure is retained to solve the problem in the thickness direction. This is done through a 2D FE discretization of the mechanical displacements and electric potential on the plate reference plane only and the mixed SSM is used to compute the through-the-thickness distributions of the dependent variables. The proposed approach is then used to compute the 3D static solutions of piezoelectric multi-layered composite plates with symmetric and anti-symmetric lamination

schemes as well as non-standard edges BC of cantilever type. Both sensor and actuator configurations are analysed and some tabulated results are given for future reference in view of validating other numerical solutions. It is worthy to mention that the validation benchmarks choice is guided by the need to show that the proposed new semi-analytic FE-state space symplectic Hamiltonian methodology can solve problems of realistic BC, multilayer composites layups and electromechanical loads other than the classical SS, cross-ply and trigonometric ones, which are the limitations of earlier semi-analytic and analytic proposed 3D solutions in the open literature. This can be seen as another original contribution of the present work.

The chapter is structured in four subsequent sections. First, Sect. 2.2 describes the in-hand problem and related notations. Then, Sect. 2.3 is devoted to the derivation of the new mixed Hamiltonian semi-analytical solution. Next, Sect. 2.4 provides few benchmarking examples to illustrate the effectiveness of the presented approach. Finally, conclusions and perspectives close the chapter.

2.2 Problem and Notations

Consider a 3D linear piezoelectric body that occupies a simply connected domain Ω to which a Cartesian global coordinate system (O,x,y,z) is attached. It is bounded by a sufficiently regular surface $\Gamma = \partial\Omega$, with outward unit vector $\underline{\mathbf{n}}$, and is subjected to a known surface traction vector $\underline{\mathbf{F}}$ on Γ_F and a scalar electric surface charge Q on Γ_Q, where Γ_F and Γ_Q are parts of its boundary Γ. The latter can also support an imposed scalar electric potential $\tilde{\varphi}$ on Γ_φ, so that $\Gamma_\varphi \cup \Gamma_Q = \Gamma$ and $\Gamma_\varphi \cap \Gamma_Q = \emptyset$, and a mechanical displacements vector $\underline{\tilde{\mathbf{u}}}$ on Γ_u, so that $\Gamma_u \cup \Gamma_F = \Gamma$ and $\Gamma_u \cap \Gamma_F = \emptyset$. For simplicity, the body loads are not considered. Besides, in the following, an underlined variable represents a vector while a doubled underlined one is used for a matrix. Also a tilted quantity is an applied (imposed) one and a bold parameter represents a tensor.

The electromechanical equations, describing the above stated static problem, are (Benjeddou, 2000) the:

- Cauchy's and Gauss' equilibrium equations

$$\begin{cases} \mathrm{Div}\boldsymbol{\sigma} = \underline{\mathbf{0}} \\ \mathrm{Div}\underline{\mathbf{D}} = 0 \end{cases} \quad \text{in} \quad \Omega \tag{2.1}$$

  where $\boldsymbol{\sigma}$ and $\underline{\mathbf{D}}$ are the Cauchy linear stress tensor and electric displacement (induction) vector. 'Div' represents the divergence operator.
- Mechanical strains-displacements and electric fields-potential relations

$$\begin{cases} \boldsymbol{\varepsilon} = \dfrac{1}{2}\left(\mathrm{Grad}\underline{\mathbf{u}} + \mathrm{Grad}^T\underline{\mathbf{u}}\right) \\ \underline{\mathbf{E}} = -\mathrm{Grad}\varphi \end{cases} \quad \text{in} \quad \Omega \tag{2.2}$$

with $\boldsymbol{\varepsilon}$ and $\underline{\mathbf{E}}$ being the engineering Lagrange linear strain tensor and electric field vector. $\underline{\mathbf{u}}$ and φ are the mechanical displacements vector and electric potential. 'Grad' denotes the gradient operator.

- Converse and direct e-form piezoelectric constitutive equations

$$\begin{cases} \underline{\boldsymbol{\sigma}} = \underline{\underline{\mathbf{C}}}^{E}\,\underline{\boldsymbol{\varepsilon}} - \underline{\underline{\mathbf{e}}}^{T}\,\underline{\mathbf{E}} \\ \underline{\mathbf{D}} = \underline{\underline{\mathbf{e}}}\,\underline{\boldsymbol{\varepsilon}} + \underline{\underline{\boldsymbol{\epsilon}}}^{\varepsilon}\,\underline{\mathbf{E}} \end{cases} \quad \text{in} \quad \Omega \tag{2.3}$$

where $\underline{\underline{\mathbf{C}}}^{E}$, $\underline{\underline{\mathbf{e}}}$ and $\underline{\underline{\boldsymbol{\epsilon}}}^{\varepsilon}$ are the elastic stiffness (at constant electric field), stress piezoelectric and dielectric (at constant strains) matrices; here, $\underline{\boldsymbol{\sigma}}$ and $\underline{\boldsymbol{\varepsilon}}$ are the engineering (in the Voigt notations) stress and strain vectors.

- Dirichlet (essential) BC

$$\begin{cases} \underline{\mathbf{u}} = \underline{\tilde{\mathbf{u}}} & \text{on } \Gamma_u \\ \varphi = \tilde{\varphi} & \text{on } \Gamma_\varphi \end{cases} \tag{2.4}$$

- Neumann (natural) BC

$$\begin{cases} \underline{\underline{\boldsymbol{\sigma}}}\,\underline{\mathbf{n}} = \underline{\mathbf{F}} & \text{on } \Gamma_F \\ \underline{\mathbf{D}}^{T}\,\underline{\mathbf{n}} = -Q & \text{on } \Gamma_Q \end{cases} \tag{2.5}$$

where $\underline{\underline{\boldsymbol{\sigma}}}$ is the matrix representing the stress tensor.

In order to formulate the reference problem in a generalized way, the following generalized displacement $\underline{\mathbf{U}}$, strain $\underline{\mathbf{S}}$, stress $\underline{\mathbf{T}}$ and load $\underline{\mathbf{G}}$ vectors are introduced (Benjeddou and Andrianarison, 2005)

$$\underline{\mathbf{U}} = \begin{Bmatrix} \underline{\mathbf{u}} \\ \varphi \end{Bmatrix}; \; \underline{\mathbf{S}} = \begin{Bmatrix} \underline{\boldsymbol{\varepsilon}} \\ -\underline{\mathbf{E}} \end{Bmatrix}; \; \underline{\mathbf{T}} = \begin{Bmatrix} \underline{\boldsymbol{\sigma}} \\ \underline{\mathbf{D}} \end{Bmatrix}; \; \underline{\mathbf{G}} = \begin{Bmatrix} \underline{\mathbf{F}} \\ -Q \end{Bmatrix} \tag{2.6}$$

As a consequence, the piezoelectric constitutive equations (2.3) rewrite as this generalized Hooke's elastic law-like form

$$\underline{\mathbf{T}} = \underline{\underline{\mathbf{C}}}\,\underline{\mathbf{S}} \tag{2.7}$$

with $\underline{\underline{\mathbf{C}}}$ being the constitutive behaviour generalized matrix (Andrianarison and Benjeddou, 2012).

It should be noticed that the negative sign before the electric field in the generalized strain vector in (2.6) is introduced in order to get a symmetric piezoelectric constitutive behaviour matrix in (2.7), as the initial equations in (2.3) are not symmetric. The equilibria equations (2.1) and gradient relations (2.2) are reformulated as:

$$\begin{cases} \underline{\underline{\mathbf{L}}}^{T}\,\underline{\mathbf{T}} = \underline{\mathbf{0}} \\ \underline{\underline{\mathbf{L}}}\,\underline{\mathbf{U}} = \underline{\mathbf{S}} \end{cases} \quad \text{in} \quad \Omega \tag{2.8}$$

where $\underline{\underline{\mathbf{L}}}$ is the linear 3D derivation matrix defined as

$$\underline{\underline{\mathbf{L}}}^T = \begin{bmatrix} \partial_x & 0 & 0 & 0 & \partial_z & \partial_y & 0 & 0 & 0 \\ 0 & \partial_y & 0 & \partial_z & 0 & \partial_x & 0 & 0 & 0 \\ 0 & 0 & \partial_z & \partial_y & \partial_x & 0 & 0 & 0 & 0 \\ 0 & 0 & 0 & 0 & 0 & 0 & \partial_x & \partial_y & \partial_z \end{bmatrix}$$

with $\partial_i, i = x, y, z$ standing for partial derivation with respect to i. Moreover, the Dirichlet and Neumann BC are re-stated as:

$$\begin{cases} \underline{\mathbf{U}} = \underline{\tilde{\mathbf{U}}} & \text{on } \Gamma_U = \Gamma_u \cup \Gamma_\varphi \\ \underline{\underline{\mathbf{T}}}\,\underline{\mathbf{n}} = \underline{\mathbf{G}} & \text{on } \Gamma_G = \Gamma_F \cup \Gamma_Q \end{cases} \tag{2.9}$$

Here, the generalized stress tensor 4th order matrix $\underline{\underline{\mathbf{T}}}$ is so that $\underline{\underline{\mathbf{T}}}^T = \left[\underline{\underline{\boldsymbol{\sigma}}} \quad \underline{\mathbf{D}}\right]$.

In summary, the strong form linear static BVP in hand was reduced to find $\underline{\mathbf{U}}$ that satisfies Eqs. (2.7)-(2.9). Worth noticeable is that for practical problems having complex geometries, loadings and BC, closed-form solutions to this BVP are unreachable. Hence, numerical solution techniques, built in the framework of VF, are necessary.

2.3 New Mixed Hamiltonian Semi-analytical Solution

In the context of multilayer composite structures modelling, the issue of enforcement of the IC conditions is a difficult task. Straightforward fulfilment of the transverse stresses and electric displacement IC constraints at the laminate interfaces is usually done in the framework of a mixed VF. Therefore, thanks to a partial Legendre transformation, a four-field *partial-mixed* VF has been established (Andrianarison and Benjeddou, 2012) so that it inherits the algebraic properties of Hamiltonian matrices, making easy its numerical implementation. However, the detailed inspection of this partial-mixed VF shows that it suffers from inconsistencies when dealing with arbitrary BC. Namely, one can show that for BC other than SS, there is not any more a one to one correspondence between the primary and conjugate nodal variables to be constrained at the discretized level. Hence, in order to overcome this drawback, the here developed approach follows two steps: in the first one, the classical generalized displacement-type VF is stated at the continuum level; then, the FE discretization and enforcement of the prescribed *essential* BC are made for the mechanical *displacements* and *electric potential*. In the second step, the Hamiltonian formalism and Legendre transformation are used to recast the Lagrange formulation into a mixed one so that the mixed SSM can be used to deal with the IC constraints enforcement at the layered composite interfaces.

The starting point in the derivation of the new VF is to state that the linear generalized constitutive equation (2.7) is resulting from this generalized quadratic strain energy density $\mathscr{E}(\underline{\mathbf{S}})$

$$\mathscr{E}(\underline{\mathbf{S}}) = \frac{1}{2}\underline{\mathbf{S}}^T \underline{\underline{\mathbf{C}}}\,\underline{\mathbf{S}} \tag{2.10}$$

through this derivation with respect to the generalized strains vector

$$\underline{\mathbf{T}} = \frac{\mathrm{d}\mathscr{E}}{\mathrm{d}\underline{\mathbf{S}}} \tag{2.11}$$

Then, the Lagrange functional associated to Eqs. (2.8)-(2.9) is defined as

$$\mathbb{L}(\underline{\mathbf{U}}) = \int_{\Omega} \mathscr{E}(\underline{\mathbf{S}}) d\Omega - \int_{\Gamma_G} \underline{\mathbf{U}}^T \underline{\mathbf{G}} d\Gamma \tag{2.12}$$

and has to be stationary for the admissible solutions

$$\int_{\Omega} \delta\mathscr{E}(\underline{\mathbf{U}}) d\Omega - \int_{\Gamma_G} \delta\underline{\mathbf{U}}^T \underline{\mathbf{G}} d\Gamma = 0 \tag{2.13}$$

Usual techniques of variational calculus can be used to show that Eq. (2.13) enforces Eqs. (2.7)-(2.8) as Euler-Lagrange equations as well as Neumann BC $(2.9)_b$ as natural ones provided that the enlarged displacement vector $\underline{\mathbf{U}}$ is searched as kinematically admissible on Γ_U i.e. $\underline{\mathbf{U}} = \underline{\tilde{\mathbf{U}}}$ on Γ_U (essential BC).

In the case of a layered body with adjoining laminae perfectly bonded together and without internal electrodes, the generalized displacement vector,

$$\underline{\mathbf{U}} = \left\{u_x, u_y, u_z, \varphi\right\}^T,$$

and transverse surface traction vector,

$$\underline{\mathbf{T}}_z = \left\{\sigma_{xz}, \sigma_{yz}, \sigma_{zz}, D_z\right\}^T,$$

should be continuous through the laminate interfaces so that these IC conditions hold

$$\left[\underline{\mathbf{U}}\right] = \underline{\mathbf{0}}\,;\ \left[\underline{\mathbf{T}}_z\right] = \underline{\mathbf{0}} \tag{2.14}$$

with $[*]$ denoting the jump in the value of the enclosed quantity * across an interface.

Now, following the procedure described in Andrianarison and Benjeddou (2012), the generalized strains vector (2.8) is split into thickness (z),

$$\mathbf{S}_z = \left\{\gamma_{xz}, \gamma_{yz}, \varepsilon_{zz}, -E_z\right\}^T$$

and in-plane (p),

$$\underline{\mathbf{S}}_p = \left\{\varepsilon_{xx}, \varepsilon_{yy}, \gamma_{xy}, -E_x, -E_y\right\}^T,$$

contributions as

$$\underline{\mathbf{S}}_z = \dot{\underline{\mathbf{U}}} + \underline{\underline{\mathbf{D}}}_1 \underline{\mathbf{U}}\ ;\ \underline{\mathbf{S}}_p = \underline{\underline{\mathbf{D}}}_2 \underline{\mathbf{U}} \tag{2.15}$$

where

$$\dot{\underline{\mathbf{U}}} = \frac{\partial \underline{\mathbf{U}}}{\partial z}; \quad \underline{\underline{\mathbf{D}}}_1 = \begin{bmatrix} 0 & 0 & \partial_x & 0 \\ 0 & 0 & \partial_y & 0 \\ 0 & 0 & 0 & 0 \\ 0 & 0 & 0 & 0 \end{bmatrix}; \quad \underline{\underline{\mathbf{D}}}_2 = \begin{bmatrix} \partial_x & 0 & 0 & 0 \\ 0 & \partial_y & 0 & 0 \\ \partial_y & \partial_x & 0 & 0 \\ 0 & 0 & 0 & \partial_x \\ 0 & 0 & 0 & \partial_y \end{bmatrix}$$

Next, the above partition leads to this similar decomposition of the generalized piezoelectric constitutive equation (2.7)

$$\begin{Bmatrix} \underline{\mathbf{T}}_p \\ \underline{\mathbf{T}}_z \end{Bmatrix} = \begin{bmatrix} \underline{\underline{\mathbf{C}}}_{pp} & \underline{\underline{\mathbf{C}}}_{pz} \\ \underline{\underline{\mathbf{C}}}_{pz}^T & \underline{\underline{\mathbf{C}}}_{zz} \end{bmatrix} \begin{Bmatrix} \underline{\mathbf{S}}_p \\ \underline{\mathbf{S}}_z \end{Bmatrix} \tag{2.16}$$

with

$$\underline{\mathbf{T}}_p = \left\{\sigma_{xx}, \sigma_{yy}, \sigma_{xy}, D_x, D_y\right\}^T$$

standing for the in-plane generalized stress vector. It should be noticed here that the original generalized Hooke's matrix coefficients of Eq. (2.7) need to be reorganized in compliance with components re-ordering for defining the in-plane and thickness generalized strain and stress vectors used in Eqs. (2.15)-(2.16).

Now, substituting Eq. (2.16) into (2.10), and having in mind generalized strains-displacements relation (2.8), provides this decomposed generalized strain energy density into thickness, in-plane and their coupling contributions

$$\mathscr{E}(\underline{\mathbf{U}}, \dot{\underline{\mathbf{U}}}) = \frac{1}{2}\left[\underline{\mathbf{S}}_p^T \underline{\underline{\mathbf{C}}}_{pp} \underline{\mathbf{S}}_p + 2\underline{\mathbf{S}}_p^T \underline{\underline{\mathbf{C}}}_{pz} \underline{\mathbf{S}}_z + \underline{\mathbf{S}}_z^T \underline{\underline{\mathbf{C}}}_{zz} \underline{\mathbf{S}}_z\right] \tag{2.17}$$

After that, when considering the thickness and in-plane partitions of the generalized strains, as in Eq. (2.15), this explicit expression of (2.17) is obtained

$$\begin{aligned} \mathscr{E}(\underline{\mathbf{U}}, \dot{\underline{\mathbf{U}}}) = {} & \frac{1}{2}\underline{\mathbf{U}}^T \underline{\underline{\mathbf{D}}}_2^T \underline{\underline{\mathbf{C}}}_{pp} \underline{\underline{\mathbf{D}}}_2 \underline{\mathbf{U}} + \underline{\mathbf{U}}^T \underline{\underline{\mathbf{D}}}_2^T \underline{\underline{\mathbf{C}}}_{pz} \underline{\underline{\mathbf{D}}}_1 \underline{\mathbf{U}} + \frac{1}{2}\underline{\mathbf{U}}^T \underline{\underline{\mathbf{D}}}_1^T \underline{\underline{\mathbf{C}}}_{zz} \underline{\underline{\mathbf{D}}}_1 \underline{\mathbf{U}} \\ & + \underline{\mathbf{U}}^T \underline{\underline{\mathbf{D}}}_2^T \underline{\underline{\mathbf{C}}}_{pz} \dot{\underline{\mathbf{U}}} + \underline{\mathbf{U}}^T \underline{\underline{\mathbf{D}}}_1^T \underline{\underline{\mathbf{C}}}_{zz} \dot{\underline{\mathbf{U}}} + \frac{1}{2}\dot{\underline{\mathbf{U}}}^T \underline{\underline{\mathbf{C}}}_{zz} \dot{\underline{\mathbf{U}}} \end{aligned} \tag{2.18}$$

And the variational equation (2.13) becomes

$$\int_{\Omega} \delta \mathscr{E}(\underline{\mathbf{U}}, \dot{\underline{\mathbf{U}}}) d\Omega - \int_{\Gamma_G} \delta \underline{\mathbf{U}}^T \underline{\mathbf{G}} d\Gamma = 0 \tag{2.19}$$

The generalized displacements are now postulated in this separated in-plane (x, y) and thickness (z) coordinates dependence

$$\underline{\mathbf{U}}(x, y, z) = \underline{\underline{\mathbf{N}}}(x, y) \underline{\mathbf{U}}^*(z) \tag{2.20}$$

where, the 2D shape functions of the in-plane interpolation matrix, $\underline{\underline{\mathbf{N}}}(x,y)$, are constructed in practice using the well-known isoparametric Lagrange interpolation and the nodal amplitudes, $\underline{\mathbf{U}}^*(z)$, are to be determined.

Similarly, the body domain and its boundary can be separated, respectively, as $\Omega(x,y,z) = \Sigma_p(x,y) \times \Sigma_z$ and $\Gamma_G = \Sigma_p^G \times \partial\Sigma_z$ with $\Sigma_z = [z_b, z_t]$ referring to the whole thickness having z_b and z_t as bottom and top coordinates. This allows to rewrite the VF (2.19) as

$$\delta \int_{\Sigma_z} \left[\frac{1}{2} \underline{\mathbf{U}}^{*T} \left(\underline{\underline{\mathbf{K}}}_1 + \underline{\underline{\mathbf{K}}}_4 + 2\underline{\underline{\mathbf{K}}}_6 \right) \underline{\mathbf{U}}^* + \underline{\mathbf{U}}^{*T} \left(\underline{\underline{\mathbf{K}}}_3 + \underline{\underline{\mathbf{K}}}_5 \right) \dot{\underline{\mathbf{U}}}^* + \frac{1}{2} \dot{\underline{\mathbf{U}}}^{*T} \underline{\underline{\mathbf{K}}}_2 \dot{\underline{\mathbf{U}}}^* + \right] dz$$
$$- \left[\delta \underline{\mathbf{U}}^{*T} \widehat{\underline{\mathbf{L}}} \right]_{z_b}^{z_t} = 0 \tag{2.21}$$

where

$$\dot{\underline{\mathbf{U}}}^* = \frac{\mathrm{d}\underline{\mathbf{U}}^*}{\mathrm{d}z}$$

and the pre-integrated in-plane matrices and vector are

$$\underline{\underline{\mathbf{K}}}_1 = \int_{\Sigma_p} \underline{\underline{\mathbf{N}}}^T \underline{\underline{\mathbf{D}}}_2^T \underline{\underline{\mathbf{C}}}_{pp} \underline{\underline{\mathbf{D}}}_2 \underline{\underline{\mathbf{N}}} d\Sigma \qquad \underline{\underline{\mathbf{K}}}_2 = \int_{\Sigma_p} \underline{\underline{\mathbf{N}}}^T \underline{\underline{\mathbf{C}}}_{zz} \underline{\underline{\mathbf{N}}} d\Sigma$$
$$\underline{\underline{\mathbf{K}}}_3 = \int_{\Sigma_p} \underline{\underline{\mathbf{N}}}^T \underline{\underline{\mathbf{D}}}_1^T \underline{\underline{\mathbf{C}}}_{zz} \underline{\underline{\mathbf{N}}} d\Sigma \qquad \underline{\underline{\mathbf{K}}}_4 = \int_{\Sigma_p} \underline{\underline{\mathbf{N}}}^T \underline{\underline{\mathbf{D}}}_1^T \underline{\underline{\mathbf{C}}}_{zz} \underline{\underline{\mathbf{D}}}_1 \underline{\underline{\mathbf{N}}} d\Sigma$$
$$\underline{\underline{\mathbf{K}}}_5 = \int_{\Sigma_p} \underline{\underline{\mathbf{N}}}^T \underline{\underline{\mathbf{D}}}_2^T \underline{\underline{\mathbf{C}}}_{pz} \underline{\underline{\mathbf{N}}} d\Sigma \qquad \underline{\underline{\mathbf{K}}}_6 = \int_{\Sigma_p} \underline{\underline{\mathbf{N}}}^T \underline{\underline{\mathbf{D}}}_2^T \underline{\underline{\mathbf{C}}}_{pz} \underline{\underline{\mathbf{D}}}_1 \underline{\underline{\mathbf{N}}} d\Sigma$$
$$\widehat{\underline{\mathbf{L}}} = \int_{\Sigma_p^G} \underline{\underline{\mathbf{N}}}^T \underline{\mathbf{G}} d\Sigma \tag{2.22}$$

Now, performing an integration by parts with respect to the nodal variables $\delta\dot{\underline{\mathbf{U}}}^*(z)$ and allowing the resulting variational equation to be satisfied for arbitrary virtual nodal variables $\delta\underline{\mathbf{U}}^*$, this second-order ODE system is obtained

$$\begin{cases} -\underline{\underline{\mathbf{K}}}_2 \ddot{\underline{\mathbf{U}}}^* + \left(\underline{\underline{\mathbf{K}}}_3 + \underline{\underline{\mathbf{K}}}_5 - \underline{\underline{\mathbf{K}}}_3^T - \underline{\underline{\mathbf{K}}}_5^T \right) \dot{\underline{\mathbf{U}}}^* + \left(\underline{\underline{\mathbf{K}}}_1 + \underline{\underline{\mathbf{K}}}_4 + \underline{\underline{\mathbf{K}}}_6 + \underline{\underline{\mathbf{K}}}_6^T \right) \underline{\mathbf{U}}^* = \underline{\mathbf{0}} \\ \underline{\underline{\mathbf{K}}}_2 \dot{\underline{\mathbf{U}}}^* + \left(\underline{\underline{\mathbf{K}}}_3^T + \underline{\underline{\mathbf{K}}}_5^T \right) \underline{\mathbf{U}}^* = \widehat{\underline{\mathbf{L}}} \qquad \text{for } z = \{z_b, z_t\} \end{cases} \tag{2.23}$$

As can be seen from Eq. (2.23), the quantity

$$\widehat{\underline{\mathbf{L}}}^* = \underline{\underline{\mathbf{K}}}_2 \dot{\underline{\mathbf{U}}}^* + \left(\underline{\underline{\mathbf{K}}}_3^T + \underline{\underline{\mathbf{K}}}_5^T \right) \underline{\mathbf{U}}^*$$

can be formally assimilated to a *nodal generalized stress vector resultant* thanks to the definition of the load vector $\widehat{\underline{\mathbf{L}}}$. It is also to be noticed that the essential BC have

been enforced at this stage and $\underline{\mathbf{U}}^*(z)$ now refers to the unconstrained degrees of freedom (DOF). The system of coupled ODE (2.23) can usually be solved in the framework of quadratic eigenvalue problem of gyroscopic type through a standard linearisation procedure which leads to a first-order ODE. However, to obtain the latter, a more systematic and elegant approach based on Legendre-Fenchel transformation of Hamiltonian systems is here adopted. For this purpose, the construction of the extended mixed Hamiltonian formulation first requires the determination of the dual or conjugate variable associated to $\dot{\underline{\mathbf{U}}}^*$. This is achieved by deriving this discretized generalized energy density, already used in the VF (2.21),

$$\mathscr{E}^*(\underline{\mathbf{U}}^*,\dot{\underline{\mathbf{U}}}^*) = \frac{1}{2}\underline{\mathbf{U}}^{*T}\left(\underline{\underline{\mathbf{K}}}_1 + \underline{\underline{\mathbf{K}}}_4 + 2\underline{\underline{\mathbf{K}}}_6\right)\underline{\mathbf{U}}^* + \underline{\mathbf{U}}^{*T}\left(\underline{\underline{\mathbf{K}}}_3 + \underline{\underline{\mathbf{K}}}_5\right)\dot{\underline{\mathbf{U}}}^* + \frac{1}{2}\dot{\underline{\mathbf{U}}}^{*T}\underline{\underline{\mathbf{K}}}_2\dot{\underline{\mathbf{U}}}^* \quad (2.24)$$

with respect to $\dot{\underline{\mathbf{U}}}^*$ so that the conjugate variable $\underline{\mathbf{P}}_z^*$ has this expression

$$\underline{\mathbf{P}}_z^* = \frac{\partial \mathscr{E}^*}{\partial \dot{\underline{\mathbf{U}}}^*} = \underline{\underline{\mathbf{K}}}_2\dot{\underline{\mathbf{U}}}^* + \left(\underline{\underline{\mathbf{K}}}_3^T + \underline{\underline{\mathbf{K}}}_5^T\right)\underline{\mathbf{U}}^* \quad (2.25)$$

By replacing the matrices in (2.25) by their expressions obtained after (2.22), it is easy to show that the conjugate nodal variables vector $\underline{\mathbf{P}}_z^*$ actually coincides with the *out-of-plane nodal transverse stresses resultant*, namely

$$\begin{aligned}\underline{\mathbf{P}}_z^* &= \int_{\Sigma_p}\left[\underline{\underline{\mathbf{N}}}^T\left(\underline{\underline{\mathbf{C}}}_{zz}\underline{\underline{\mathbf{N}}}\dot{\underline{\mathbf{U}}}^* + \underline{\underline{\mathbf{C}}}_{zz}\underline{\underline{\mathbf{N}}}\underline{\underline{\mathbf{D}}}_1\underline{\mathbf{U}}^* + \underline{\underline{\mathbf{C}}}_{pz}^T\underline{\underline{\mathbf{N}}}\underline{\underline{\mathbf{D}}}_2\underline{\mathbf{U}}^*\right)\right]d\Sigma \\ &= \int_{\Sigma_p}\underline{\underline{\mathbf{N}}}^T\left(\underline{\underline{\mathbf{C}}}_{pz}^T\underline{\mathbf{S}}_p + \underline{\underline{\mathbf{C}}}_{zz}\underline{\mathbf{S}}_z\right)d\Sigma \\ &\equiv \int_{\Sigma_p}\underline{\underline{\mathbf{N}}}(x,y)^T\underline{\mathbf{T}}_z\,d\Sigma \end{aligned} \quad (2.26)$$

Next, Eq. (2.25) is solved for $\dot{\underline{\mathbf{U}}}^*$ so that:

$$\dot{\underline{\mathbf{U}}}^* = \underline{\underline{\mathbf{K}}}_2^{-1}\underline{\mathbf{P}}_z^* - \underline{\underline{\mathbf{K}}}_2^{-1}\left(\underline{\underline{\mathbf{K}}}_3^T + \underline{\underline{\mathbf{K}}}_5^T\right)\underline{\mathbf{U}}^* \quad (2.27)$$

Now, the elimination of $\dot{\underline{\mathbf{U}}}^*$ from the generalized strain energy density functional (2.24), combined with a Legendre transformation defined as,

$$\mathscr{H}^*(\underline{\mathbf{U}}^*,\underline{\mathbf{P}}_z^*) = \underline{\mathbf{P}}_z^{*T}\dot{\underline{\mathbf{U}}}^* - \mathscr{E}^*(\underline{\mathbf{U}}^*,\dot{\underline{\mathbf{U}}}^*) \quad (2.28)$$

leads to this explicit expression of the earlier Hamiltonian energy density functional

$$\begin{aligned}\mathscr{H}^*(\underline{\mathbf{U}}^*,\underline{\mathbf{P}}_z^*) = &\frac{1}{2}\underline{\mathbf{P}}_z^{*T}\underline{\underline{\mathbf{K}}}_2^{-1}\underline{\mathbf{P}}_z^* - \underline{\mathbf{P}}_z^{*T}\underline{\underline{\mathbf{K}}}_2^{-1}(\underline{\underline{\mathbf{K}}}_3^T + \underline{\underline{\mathbf{K}}}_5^T)\underline{\mathbf{U}}^* \\ &- \frac{1}{2}\underline{\mathbf{U}}^{*T}\left[\underline{\underline{\mathbf{K}}}_1 + \underline{\underline{\mathbf{K}}}_4 + \underline{\underline{\mathbf{K}}}_6 + \underline{\underline{\mathbf{K}}}_6^T - (\underline{\underline{\mathbf{K}}}_3 + \underline{\underline{\mathbf{K}}}_5)\underline{\underline{\mathbf{K}}}_2^{-1}(\underline{\underline{\mathbf{K}}}_3^T + \underline{\underline{\mathbf{K}}}_5^T)\underline{\mathbf{U}}^*\right]\end{aligned} \tag{2.29}$$

Thus, using (2.28), the Lagrangian VF (2.21) transforms into this Hamiltonian one

$$\delta\int_{\Sigma_z}\left[\underline{\mathbf{P}}_z^{*T}\dot{\underline{\mathbf{U}}}^* - \mathscr{H}^*(\underline{\mathbf{U}}^*,\underline{\mathbf{P}}_z^*)\right]dz - \left[\delta\underline{\mathbf{U}}^{*T}\widehat{\underline{\mathbf{L}}}\right]_{z_b}^{z_t} = 0 \tag{2.30}$$

Now, expliciting the variation in (2.30), combined with an integration by parts with regards to $\delta\dot{\underline{\mathbf{U}}}^*$, gives

$$\int_{\Sigma_z}\left[\delta\underline{\mathbf{P}}_z^{*T}\dot{\underline{\mathbf{U}}} - \delta\underline{\mathbf{U}}^{*T}\dot{\underline{\mathbf{P}}}_z - \delta\underline{\mathbf{U}}^{*T}\left(\frac{\partial\mathscr{H}^*}{\partial\underline{\mathbf{U}}^*}\right) - \delta\underline{\mathbf{P}}_z^{*T}\left(\frac{\partial\mathscr{H}^*}{\partial\underline{\mathbf{P}}_z^{*T}}\right)\right]dz + \left[\delta\underline{\mathbf{U}}^{*T}\left(\underline{\mathbf{P}}_z^* - \widehat{\underline{\mathbf{L}}}\right)\right]_{z_b}^{z_t} = 0 \tag{2.31}$$

After grouping together the terms relative to the same virtual nodal variables, the previous equation turns into the following one

$$\begin{aligned}&\int_{\Sigma_z}\delta\underline{\mathbf{U}}^{*T}\left(-\dot{\underline{\mathbf{P}}}^* - \frac{\partial\mathscr{H}^*}{\partial\underline{\mathbf{U}}^*}\right)d\Sigma_z + \int_{\Sigma_z}\delta\underline{\mathbf{P}}_z^{*T}\left(\dot{\underline{\mathbf{U}}}^* - \frac{\partial\mathscr{H}^*}{\partial\underline{\mathbf{P}}_z^*}\right)dz = 0 \\ &\forall\left(\delta\underline{\mathbf{U}}^*,\delta\underline{\mathbf{P}}_z^*\right)/\underline{\mathbf{P}}_z^* = \widehat{\underline{\mathbf{L}}} \quad \text{on } z = \{z_b, z_t\}\end{aligned} \tag{2.32}$$

Now, the expression (2.29) of $\mathscr{H}^*$ is substituted in Equation (2.32), leading to

$$\begin{aligned}\sum_{k=1}^{k=\mathrm{NL}}\int_{z_k}^{z_{k+1}}&\left[\delta\underline{\mathbf{P}}_z^{*T}\dot{\underline{\mathbf{U}}}^* - \delta\underline{\mathbf{U}}^{*T}\dot{\underline{\mathbf{P}}}_z^* + \delta\underline{\mathbf{U}}^{*T}\left(\underline{\underline{\mathbf{B}}}_k\underline{\mathbf{U}}^* + \underline{\underline{\mathbf{A}}}_k^T\underline{\mathbf{P}}_z^*\right)\right. \\ &\left.+\delta\underline{\mathbf{P}}_z^{*T}\left(-\underline{\underline{\mathbf{D}}}_k\underline{\mathbf{P}}_z^* + \underline{\underline{\mathbf{A}}}_k\underline{\mathbf{U}}^*\right)\right]dz = 0\end{aligned} \tag{2.33}$$

where, NL is the number of layers and the layer-dependent matrices are given by

$$\begin{aligned}&\underline{\underline{\mathbf{D}}}_k = \underline{\underline{\mathbf{K}}}_2^{-1} \quad ; \quad \underline{\underline{\mathbf{A}}}_k = \underline{\underline{\mathbf{K}}}_2^{-1}\left(\underline{\underline{\mathbf{K}}}_3^T + \underline{\underline{\mathbf{K}}}_5^T\right) \\ &\underline{\underline{\mathbf{B}}}_k = \underline{\underline{\mathbf{K}}}_1 + \underline{\underline{\mathbf{K}}}_4 + \underline{\underline{\mathbf{K}}}_6 + \underline{\underline{\mathbf{K}}}_6^T - \left(\underline{\underline{\mathbf{K}}}_3 + \underline{\underline{\mathbf{K}}}_5\right)\underline{\underline{\mathbf{K}}}_2^{-1}\left(\underline{\underline{\mathbf{K}}}_3^T + \underline{\underline{\mathbf{K}}}_5^T\right)\end{aligned}$$

Hence, thanks to the arbitrariness of $\delta\underline{\mathbf{U}}^*$ and $\delta\underline{\mathbf{P}}_z^*$, Eq. (2.33) leads to this first-order ODE system for the k-th layer

$$\begin{Bmatrix}\dot{\underline{\mathbf{U}}}^* \\ \dot{\underline{\mathbf{P}}}_z^*\end{Bmatrix} = \begin{bmatrix}-\underline{\underline{\mathbf{A}}}_k & \underline{\underline{\mathbf{D}}}_k \\ \underline{\underline{\mathbf{B}}}_k & \underline{\underline{\mathbf{A}}}_k^T\end{bmatrix}\begin{Bmatrix}\underline{\mathbf{U}}^* \\ \underline{\mathbf{P}}_z^*\end{Bmatrix} \tag{2.34}$$

It is worth mentioning from Eq. (2.34) that the number of *dual* nodal generalized stress resultants $\underline{\mathbf{P}}_z^*$ variables is now equal to the number of unconstrained *N primary* nodal generalized displacements $\underline{\mathbf{U}}^*$ ones so that Equation (2.34) is actually a *2N* linear system with *2N* unknowns. Besides, it can be readily shown that the system matrix of (2.34) is of Hamiltonian type since it satisfies the following identity for a given layer k

$$\underline{\underline{\mathbf{J}}}\,\underline{\underline{\mathbf{H}}}_k = \left(\underline{\underline{\mathbf{J}}}\,\underline{\underline{\mathbf{H}}}_k\right)^T \tag{2.35}$$

with

$$\underline{\underline{\mathbf{H}}}_k = \begin{bmatrix} -\underline{\underline{\mathbf{A}}}_k & \underline{\underline{\mathbf{D}}}_k \\ \underline{\underline{\mathbf{B}}}_k & \underline{\underline{\mathbf{A}}}_k^T \end{bmatrix}; \underline{\underline{\mathbf{J}}} = \begin{bmatrix} \underline{\underline{\mathbf{0}}} & \underline{\underline{\mathbf{I}}} \\ -\underline{\underline{\mathbf{I}}} & \underline{\underline{\mathbf{0}}} \end{bmatrix} \tag{2.36}$$

Furthermore, the diagonalization of the Hamiltonian matrix $\underline{\underline{\mathbf{H}}}_k$ is reached using the eigen solutions, $\left\{\underline{\boldsymbol{\mu}}_k; \underline{\underline{\boldsymbol{\Psi}}}_k\right\}$ of the following Hamiltonian eigenvalue problem

$$\underline{\underline{\mathbf{H}}}_k \underline{\underline{\boldsymbol{\Psi}}}_k = \underline{\underline{\boldsymbol{\Psi}}}_k \,\mathrm{Diag}\left(\underline{\boldsymbol{\mu}}_k\right) \tag{2.37}$$

As it can be noticed, $tr\left(\underline{\underline{\mathbf{H}}}_k\right) = 0$ (*tr* is the trace operator) so that the spectrum of the eigenvalue problem can be partitioned as

$$\mathrm{Diag}\left(\underline{\boldsymbol{\mu}}_k\right) = \begin{bmatrix} \mathrm{Diag}\left(\underline{\boldsymbol{\mu}}_k^+\right) & \underline{\underline{\mathbf{0}}} \\ \underline{\underline{\mathbf{0}}} & -\mathrm{Diag}\left(\underline{\boldsymbol{\mu}}_k^+\right) \end{bmatrix}; \underline{\boldsymbol{\mu}}_k^+ \in \mathbb{C}/\mathrm{Re}\left(\underline{\boldsymbol{\mu}}_k^+\right) > 0 \tag{2.38}$$

Similarly, the eigen matrix splits into two parts as

$$\underline{\underline{\boldsymbol{\Psi}}}_k = \left[\underline{\underline{\boldsymbol{\Psi}}}_k^+ \quad \underline{\underline{\boldsymbol{\Psi}}}_k^-\right] \tag{2.39}$$

Where, each of its bloc matrices satisfies the following symplectic-orthogonality relation

$$\underline{\underline{\boldsymbol{\Psi}}}_k^{i^T} \underline{\underline{\mathbf{J}}}\,\underline{\underline{\boldsymbol{\Psi}}}_k^j = -\left(\underline{\underline{\boldsymbol{\Psi}}}_k^j \underline{\underline{\mathbf{J}}}\,\underline{\underline{\boldsymbol{\Psi}}}_k^i\right)^T = \delta_{ij}\underline{\underline{\mathbf{I}}} \tag{2.40}$$

Further on, considering this generalized state vector $\underline{\mathbf{Z}}_k^* = \left\{\underline{\mathbf{U}}^* \quad \underline{\mathbf{P}}_z^*\right\}_k^T$, and making use of its modal projection as $\underline{\boldsymbol{\Pi}}_k^* = \underline{\underline{\boldsymbol{\Psi}}}_k \underline{\mathbf{Z}}_k^*$, the Hamiltonian eigenvalue problem (2.37) and the symplectic-orthogonality relation (2.40) allow to recast Eq. (2.37) into a diagonal form so that its general solution writes, for a given layer k, as

$$\underline{\mathbf{Z}}_k^* = \underline{\underline{\boldsymbol{\Psi}}}_k \,\mathrm{Diag}\left(e^{\underline{\boldsymbol{\mu}}_k z}\right) \underline{\boldsymbol{\Lambda}}_k \tag{2.41}$$

Where, the unknown layer-dependent coefficients vectors $\underline{\boldsymbol{\Lambda}}_k$ are determined with the help of the IC constraints together with the BC on top and bottom surfaces of the composite, thereby completing the resolution of Eq. (2.35). Clearly this solution is of analytic type and hence the capacity to account for the exact satisfaction of the

IC as well as the BC on the top and bottom of the composite is expected. Finally, the formulation of the problem in terms of the state vector $\underline{\mathbf{Z}}_k^*$ allows to use the well-known mixed SSM to compute the solution throughout the whole thickness. The case of a layered composite is then treated through a propagator matrix which maps the state vector on the bottom to any height while satisfying the IC and BC (see Andrianarison and Benjeddou, 2012, for more details).

2.4 Benchmarking Examples

In this section, several numerical examples are investigated to test the stability and accuracy of the proposed method. The focus is made here on open literature benchmarks that provide tabulated results for non-classical BC (cantilever), multilayer composite layups (angle-ply) and electromechanical loads (uniform). The aim is to avoid, as much as possible, graphical (curves)-induced comparison errors and exact, closed-form and earlier solutions limitations to SS BC, cross-ply composite layups and trigonometric electromechanical loads. Such classical benchmarks are abundant in the open literature and have been already analysed in an earlier work (Andrianarison and Benjeddou, 2012). It is worthy to mention that tabulated results for the above mentioned non-classical configurations are rather seldom in the open literature and related benchmarks choice is very limited. Therefore, a numerical convergence analysis is first performed through the test-case of a cantilever PVDF bimorph, that is clamped on the edge $x = 0$ and free elsewhere. The actuator configuration is furthermore considered and the results are compared with reference 3D FE solutions. Next, the assessment of the accuracy of the method is obtained by analysing the bending of a PZT angle-ply composite plate under sensor configuration for which the cantilever and SS BC are successively analysed.

Before we proceed to the presentation of the benchmarking examples, it is worthwhile to show how the BC are actually taken into account in the numerical procedure. Let us consider the case of *a sensor* configuration where a mechanical force is applied on the top surface and a zero potential is applied on both lower and upper surfaces (Fig. 2.1a). We recall that, at the final stage of the aforementioned Hamiltonian VF, a $2N$ algebraic system is obtained after the *mechanical* displacement variables are constrained in agreement with the actual lateral BC, that is

$$\begin{Bmatrix} \underline{\mathbf{u}} \\ \underline{\varphi} \\ \underline{\mathbf{P}}_m \\ \underline{\mathbf{P}}_e \end{Bmatrix}_t = \begin{bmatrix} \underline{\underline{\mathbf{H}}}_{uu} & \underline{\underline{\mathbf{H}}}_{u\varphi} & \underline{\underline{\mathbf{H}}}_{up_m} & \underline{\underline{\mathbf{H}}}_{up_e} \\ \underline{\underline{\mathbf{H}}}_{\varphi u} & \underline{\underline{\mathbf{H}}}_{\varphi\varphi} & \underline{\underline{\mathbf{H}}}_{\varphi p_m} & \underline{\underline{\mathbf{H}}}_{\varphi p_e} \\ \underline{\underline{\mathbf{H}}}_{p_m u} & \underline{\underline{\mathbf{H}}}_{p_m\varphi} & \underline{\underline{\mathbf{H}}}_{p_m p_m} & \underline{\underline{\mathbf{H}}}_{p_m p_e} \\ \underline{\underline{\mathbf{H}}}_{p_e u} & \underline{\underline{\mathbf{H}}}_{p_e\varphi} & \underline{\underline{\mathbf{H}}}_{p_e p_m} & \underline{\underline{\mathbf{H}}}_{p_e p_e} \end{bmatrix} \begin{Bmatrix} \underline{\mathbf{u}} \\ \underline{\varphi} \\ \underline{\mathbf{P}}_m \\ \underline{\mathbf{P}}_e \end{Bmatrix}_b \tag{2.42}$$

where index m (resp. e) refers to *mechanical* (resp. *electric*) type variables.

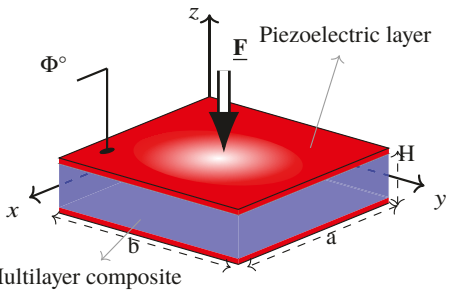

(a) Geometry and electromechanical loads of a piezoelectric multilayer composite

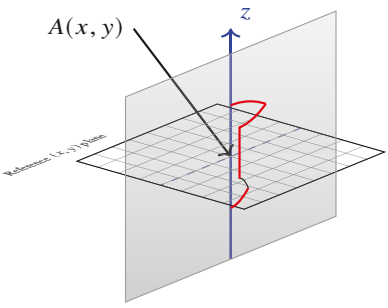

(b) Through-thickness evaluation of variables at point $A(x, y)$ of the 2D FE meshed reference plane

Fig. 2.1. Geometry and FE-SSM semi-analytical point 3D solution for a piezoelectric multilayer plate

As soon as the electric potential is fixed on the bottom and top surfaces, the second equation of (2.42) can be solved for the electric displacement nodal unknowns in terms of the mechanical nodal unknowns $\underline{\mathbf{u}}^b$ so that

$$\underline{\mathbf{P}}_e^b = \underline{\underline{\mathbf{H}}}_{\varphi p_e}^{-1} \left(\underline{\varphi}^t - \underline{\underline{\mathbf{H}}}_{\varphi u} \underline{\mathbf{u}}^b + \underline{\underline{\mathbf{H}}}_{\varphi\varphi} \underline{\varphi}^b + \underline{\underline{\mathbf{H}}}_{\varphi p_m} \underline{\mathbf{P}}_m^b \right) \tag{2.43}$$

Next, combining equation (2.43) with the third equation of (2.42) allows us to solve $\underline{\mathbf{u}}^b$ as the solution of

$$\begin{aligned} &\left(\underline{\underline{\mathbf{H}}}_{p_m u} - \underline{\underline{\mathbf{H}}}_{p_m p_e} \underline{\underline{\mathbf{H}}}_{\varphi p_e}^{-1} \underline{\underline{\mathbf{H}}}_{\varphi u} \right) \underline{\mathbf{u}}^b = \underline{\mathbf{P}}_m^t - \left(\underline{\underline{\mathbf{H}}}_{p_m p_e} - \underline{\underline{\mathbf{H}}}_{p_m p_m} \underline{\underline{\mathbf{H}}}_{\varphi p_e}^{-1} \underline{\underline{\mathbf{H}}}_{\varphi p_m} \right) \underline{\mathbf{P}}_m^b \\ &- \left(\underline{\underline{\mathbf{H}}}_{p_m \varphi} - \underline{\underline{\mathbf{H}}}_{p_m p_e} \underline{\underline{\mathbf{H}}}_{\varphi p_e}^{-1} \underline{\underline{\mathbf{H}}}_{\varphi\varphi} \right) \underline{\varphi}^b - \underline{\underline{\mathbf{H}}}_{p_m p_e} \underline{\underline{\mathbf{H}}}_{\varphi p_e}^{-1} \underline{\varphi}^t \end{aligned} \tag{2.44}$$

Once $\underline{\mathbf{u}}^b$ are determined, all other nodal variables on the lower surface are easily recovered recursively and the solution through-the-thickness of the plate is computed with the help of the propagator matrix.

2.4.1 Numerical Convergence Analysis

In this first example, a piezoelectric cantilever bimorph (Fig. 2.2) under *uniform* electric load is investigated using the proposed method. It is made of two-ply PVDF identical layers with outward opposite polarities to obtain a bending actuator. The bimorph total thickness is $h = 1$ mm whereas the length is $a = 100$ mm and the width is $b = 5$ mm. The actuator configuration is considered here so that a uniform electric potential $\bar{\Phi} = 1\,V$ is applied on the top surface. The edge BC of the bimorph are assumed clamped on the edge $x = 0$; that is $u_x|_{x=0} = u_y|_{x=0} = u_z|_{x=0} = 0$ and free

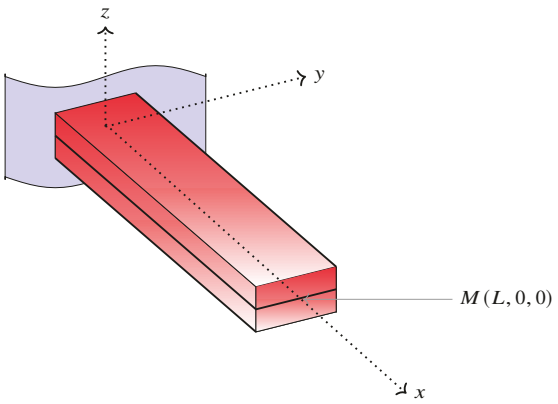

Fig. 2.2 Bimorph actuator configuration

elsewhere. The material properties of the PVDF layers used in this numerical example are (Tzou, 1993): $E_1 = E_2 = E_3 = 2\,\text{GPa}$, $\nu_{12} = \nu_{13} = \nu_{23} = 0.29$, $G_{12} = G_{13} = G_{23} = 1\,\text{GPa}$, $e_{31} = e_{32} = 0.046\,\text{C/m}^2$, $e_{33} = e_{24} = e_{15} = 0.0$, $\epsilon^S_{11} = \epsilon^S_{22} = \epsilon^S_{33} = 106.2\,\text{pF/m}$.

Some selected references are given here for comparison. The results in Tahani and Naserian-Nik (2013); Phung-Van et al (2015); Li et al (2014); Vidal et al (2011) were obtained through 3D FE, 2D plate isogeometric FE, plate B-Spline finite point and refined shell FE methods, respectively. These reference solutions are used here to analyse the behaviour of the present semi-analytical solution in terms of accuracy, stability and convergence. The variables are thus evaluated in specific in-plane locations along the bimorph where their values are compared with those obtained by the references. Therefore, the static deflection of the bimorph at those specific points are given in Table 2.1 for the here implemented Q4 FE different mesh discretizations. It can be seen that the results obtained with the present approach agree very well with the 3D FEM solution as given in Tahani and Naserian-Nik (2013) and are more accurate than those of the other 2D methods (isogeometric FE of Phung-Van et al (2015), B-spline finite point of Li et al (2014) and refined shell FE of Vidal et al (2011)). Besides, it is clear that the convergence of the present semi-analytical approach is very rapid as the reference values are reached for the five evaluation points with a maximum relative deviation of less than 1.5% using a coarse mesh of 16 (8x2) in-plane FE (Fig. 2.3). Moreover, the through-the-normalized ($Z = z/h$) thickness distributions of the non-dimensional transverse stresses

$$(\tilde{\sigma}_{xz}, \tilde{\sigma}_{zz}) = (\sigma_{xz}, \sigma_{zz}) \times \frac{a}{\bar{\Phi} e_{31}}$$

and the non-dimensional transverse electric displacement

$$\tilde{D}_z = \frac{D_z}{e_{31}} \times 10^6$$

displayed in Figs. 2.4 and 2.5 confirm that the IC constraints are satisfied.

Table 2.1
Transverse displacement ($u_z \times 10^{-7}$ m) at point (x mm, 0, 0) for a PVDF bimorph actuator

Solution method	Mesh	Point location x (mm)				
		20	40	60	80	100
Present (2D Q4 FE-SSM)	4×2	0.125	0.505	0.99	1.75	2.815
	6×2	0.131	0.532	1.140	2.054	3.210
	8×2	0.134	0.543	1.223	2.183	3.434
	10×2	0.134	0.543	1.225	2.183	3.435
	12×2	0.134	0.543	1.224	2.183	3.435
Error_{3D} (%)[b]		−1.47	−0.55	−0.65	−0.55	0.73
3D H8 FE (Tahani and Naserian-Nik, 2013)[a]	5×1×2	0.136	0.546	1.232	2.193	3.410
2D plate quadratic isogeometric FE (Phung-Van et al, 2015)	101×6	0.138	0.550	1.236	2.201	3.443
Error_{3D} (%)[b]		1.47	0.97	0.73	0.36	0.32
2D plate B-Spline finite point (Li et al, 2014)	5×4	0.137	0.551	1.241	2.207	3.449
Error_{3D} (%)[b]		0.74	0.92	0.73	0.64	1.14
2D refined shell Q8 FE Vidal et al (2011)	5×1	0.137	0.551	1.241	2.207	3.449
Error_{3D} (%)[b]		0.73	0.91	0.73	0.64	1.14

[a] The numerical values are obtained from non-dimensional quantities in Tahani and Naserian-Nik (2013)
[b] The errors are computed with respect to 3D FE results

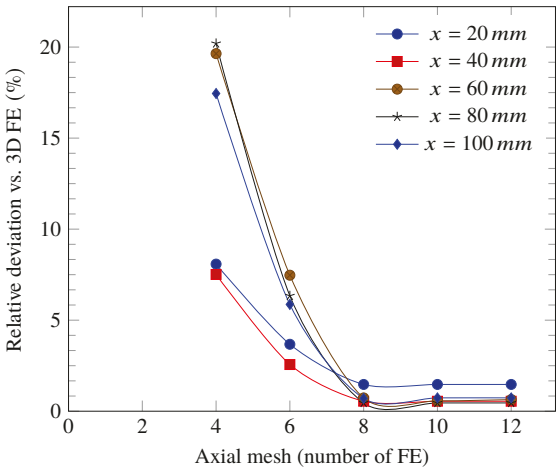

Fig. 2.3 Deflection convergence plots at different axial positions for the PVDF bimorph actuator

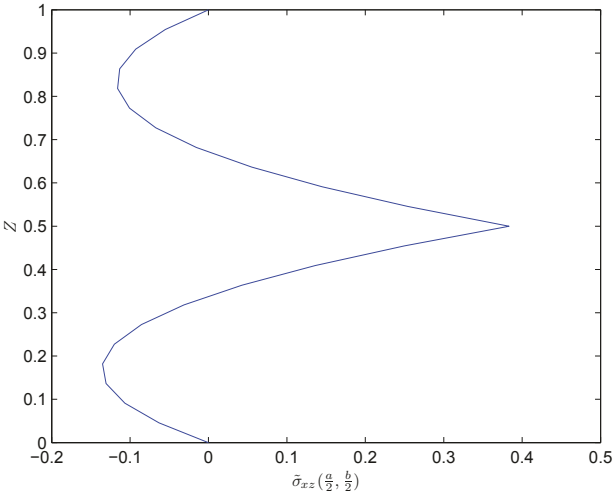

(a) Through-the-thickness distribution of $\tilde{\sigma}_{xz}$

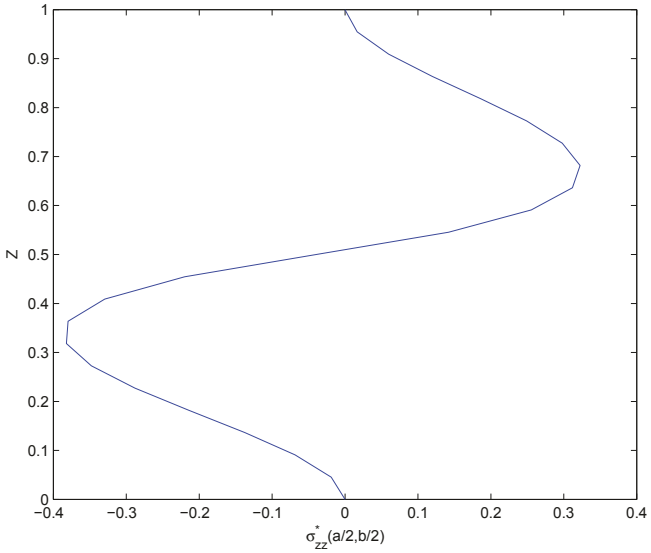

(b) Through-the-thickness distribution of $\tilde{\sigma}_{zz}$

Fig. 2.4. Through-thickness distributions of non-dimensional transverse stresses in the PVDF bimorph actuator

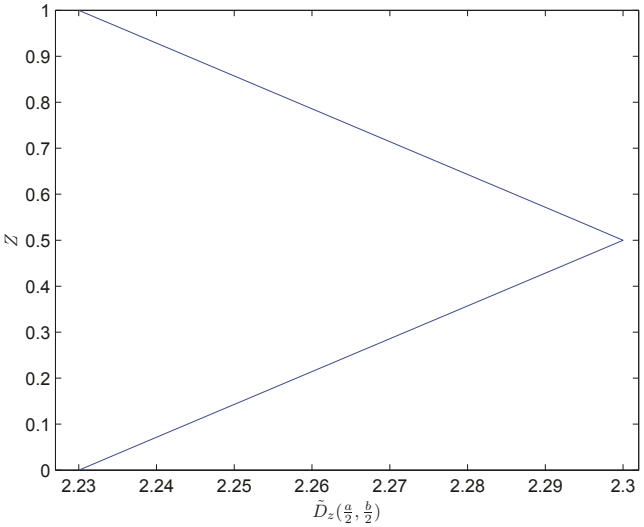

Fig. 2.5. Through-thickness distribution of $\tilde{D}_z$ in the PVDF bimorph actuator

Table 2.2 shows the results relative to the bimorph tip deflection when different voltages are applied. They are compared with those of 2D B-spline finite point approach (Li et al, 2014) and with the theoretical and experimental data provided by Tzou (1989). First, the observed relatively high deviations of the numerical results with respect to the experimental ones can be explained by the stiffer clamping BC numerical reperesentation compared to the softer actual ones, and by the non-realistic (electromechanical isotropic behaviour, nil elastic Poisson's ratio and piezoelectric

Table 2.2
Tip deflection ($u_z \times 10^{-7}$ m) of the PVDF bimorph for different applied voltages

Method	Voltage (V)					
	10	40	80	130	160	200
Present (10×2)	3.460	13.771	27.407	45.433	54.703	68.228
$\text{Error}^*_{\text{exp}}$(%)	5.33	10.48	12.37	13.06	9.22	7.91
Experiment (Tzou, 1989)	3.285	12.465	24.390	40.185	50.085	63.225
Classical beam theory (Tzou, 1989)	3.450	13.800	27.600	44.850	55.200	69.000
$\text{Error}^*_{\text{exp}}$(%)	5.02	10.71	13.16	11.61	10.21	9.13
2D B-spline finite point (Li et al, 2014)	3.449	13.797	27.794	44.841	55.188	68.986
$\text{Error}^*_{\text{exp}}$(%)	4.99	10.6	13.96	11.59	10.19	9.11

* The errors are computed with respect to the experimental results

coupling coefficients, etc.) PVDF available material data. Then, it can be seen that the results obtained with the present method match well the theoretical ones obtained in Tzou (1989) and are the closest to the experimental values, in particular for the last two highest actuation voltages (see Fig. 2.6). To assess the computational cost, a comparison of different models in terms of the number of DOF is presented in Table 2.3 when the convergence is reached. It can be observed that the present 2D Q4 FE-SSM semi-analytical 3D solution is the cheapest (lowest total DOF) and, as expected, its characteristics are closer to the 3D FE solution in terms of cost (total non-nil DOF) and accuracy (relative deviation, see Table 2.1).

Table 2.3
Computational cost (out of clamped nodes and DOF) comparison of the present 3D semi-analytic solution with others for the PVDF bimorph actuator

Method	FE	Free nodes	Mechanical (free DOF)	Electrical (non nil DOF)	Total (non nil DOF)
Present 3D semi-analytical (Q4 FE-SSM)	16	24	72	24	96
3D H8 FE (Tzou, 1993)	10	30	90	24	114
2D refined shell Q8 FE (Vidal et al, 2011)	5	25	175	10	185
2D plate B-Spline finite point (Li et al, 2014)	20	25	125	50	175

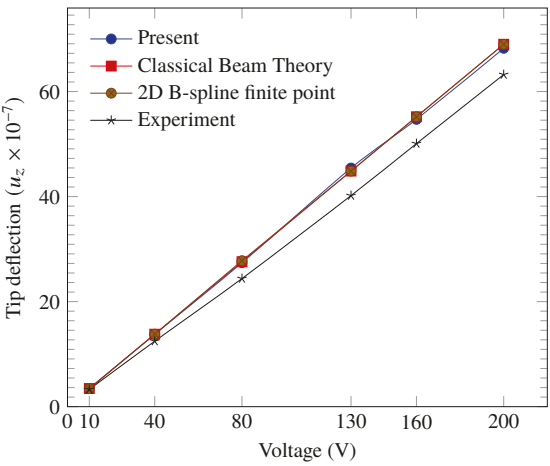

Fig. 2.6 Bimorph tip deflection under different actuation voltages

2.4.2 Square Cantilever PZT Angle-ply Composite Plate

A (20 cm × 20 cm) six-layer cantilever plate, made of T300/976 Graphite-Epoxy (GE) and piezoceramic (PZT-G1195N) materials, is considered (Pablo et al, 2009). The BC are thus $u_x|_{x=0} = u_y|_{x=0} = u_z|_{x=0} = 0$. The GE composite is bonded by PZT layers on its bottom and top surfaces and each of its laminae is of equal thickness (see Fig. 2.1a). The composite plate total thickness is fixed as $h = 1$ mm whereas that of each PZT layer is 0.1 mm. The anti-symmetric (as) laminate angle-ply sequence is considered; that is $[\mathrm{PZT}/-\theta/\theta]_{as}$ where θ (here 45°) is the fiber orientation angle of the ply. The material properties are summarized in Table 2.4. It should be noticed that the PZT-G1195N material properties given in Pablo et al (2009) are unrealistically considered as elastically isotropic whereas those in Benjeddou et al (2002) are realistically anisotropic (transverse-isotropic). The simulation is conducted for both datasets in order to show the influence of the unrealistic assumption of PZT isotropic elastic behaviour. Besides, only the sensor configuration is considered in this test-case; that is, a uniform mechanical pressure of amplitude $p^\circ = 100\,\mathrm{N/m^2}$ is applied on the upper surface whereas a zero equipotential voltage is imposed on the plate bottom and top surfaces. Table 2.5 shows that the present semi-analytical approach is able to recover, with −0.18% of relative deviation for the same mesh, the 2D FE solution (Pablo et al, 2009) based on the classical plate theory and without electric DOF. Besides, it is clear that the unrealistic behaviour assumption for the PZT-G1195N greatly overestimates its realistic anisotropic (transverse-isotropic) one. Indeed, the converged tip deflection computed using the former over estimates by

Table 2.4
Material properties of the PZT composite plate ($\epsilon^\circ = 8.85 \times 10^{-12}\mathrm{C/Nm^2}$)

	Pablo et al (2009)		Benjeddou et al (2002)		Benjeddou et al (2002)	
Property	T300/976 GE	PZT-G1195N	Property	T300/976 GE	Property	PZT-G1195N
E_1, GPa	150	63.0	E_1, GPa	150	C_{11}, GPa	148
E_2, GPa	9.0	63.0	E_2, GPa	9.0	C_{22}, GPa	148
E_3, GPa	9.0	63.0	E_3, GPa	9.0	C_{33}, GPa	131
G_{12}, GPa	7.1	24.2	G_{12}, GPa	7.1	C_{12}, GPa	76.2
G_{13}, GPa	7.1	24.2	G_{13}, GPa	7.1	C_{13}, GPa	74.2
G_{23}, GPa	2.5	24.2	G_{23}, GPa	2.5	C_{23}, GPa	74.2
ν_{12}	0.3	0.3	ν_{12}	0.30	C_{66}, GPa	35.9
ν_{23}	0.3	0.3	ν_{23}	0.30	C_{44}, GPa	25.4
ν_{13}	0.3	0.3	ν_{13}	0.30	C_{55}, GPa	25.4
d_{31}, pmV^{-1}	0.0	-254	e_{31}, C/m^2	0.0	e_{31}, C/m^2	-2.1
d_{32}, pmV^{-1}	0.0	-254	e_{32}, C/m^2	0.0	e_{32}, C/m^2	-2.1
d_{33}, pmV^{-1}	0.0	374	e_{33}, C/m^2	0.0	e_{33}, C/m^2	9.5
d_{15}, pmV^{-1}	0.0	584	e_{15}, C/m^2	0.0	e_{15}, C/m^2	9.2
d_{24}, pmV^{-1}	0.0	584	e_{24}, C/m^2	0.0	e_{24}, C/m^2	9.2
ϵ_{11}^T, nFm^{-1}	0.0	15.3	$\epsilon_{11}^S/\epsilon^\circ$	3.5	$\epsilon_{11}^S/\epsilon^\circ$	460
ϵ_{22}^T, nFm^{-1}	0.0	15.3	$\epsilon_{22}^S/\epsilon^\circ$	3.0	$\epsilon_{22}^S/\epsilon^\circ$	460
ϵ_{33}^T, nFm^{-1}	0.0	15.0	$\epsilon_{33}^S/\epsilon^\circ$	3.0	$\epsilon_{33}^S/\epsilon^\circ$	235

Table 2.5
Tip deflection u_z (mm) at point $(0.2\,\mathrm{m}, 0, 0)$ of cantilever PZT composite plate under uniform pressure

Method	Mesh	Isotropic PZT (Pablo et al, 2009)	Transverse-Isotropic PZT (Benjeddou et al, 2002)
2D plate FE (Pablo et al, 2009)	6×6	2.750^a	–
Present (2D Q4 FE-SSM)	6×6	2.745 (−0.18%)	1.408
(deviation)	8×8	2.748 (−0.07%)	1.410
	10×10	2.748 (−0.07%)	1.410

[a] This numerical value is estimated from Fig. 4 of Pablo et al (2009) and may be subjected to inaccuracies

94.89% that obtained using the latter (see the last line and column values of Table 2.5).

2.4.3 Square SS PZT Angle-ply Composite Plate

The same PZT composite plate investigated in Subsect. 2.4.2 is considered here. However, the plate is here supposed to be under SS-2 BC defined as $u_y = u_z = 0$ at $x = \{0, a\}$ and $u_x = u_z = 0$ at $y = \{0, b\}$. The PZT-G1195N electro-mechanical properties given in Table 2.4 (Pablo et al, 2009) are retained. Both symmetric (s) and anti-symmetric stacking sequences are considered; that is $[PZT/-\theta/\theta]_{as}$ and $[\mathrm{PZT}/-\theta/\theta]_s$ with $\theta = 45°$.

Table 2.6 shows that the present semi-analytical approach is able to predict accurate results with relative deviations of −0.03% for the symmetric and 0.06% for the anti-symmetric 45° stacking with regards to the meshless Radial Point Interpolation Method (RPIM) presented in Liu et al (2004). It can be also observed that the central deflection is higher for all anti-symmetric layups and increases with decreasing the ply angle. Moreover, the through-the-normalized ($Z = z/H, H = h + 2h_p$) thickness distributions of the non-dimensional transverse shear stress $\tilde{\sigma}_{xz} = \sigma_{xz} \times (H/ap^\circ)$ and

Table 2.6
Central point deflection ($\times 10^{-5} m$) of a SS PZT composite plate under uniform pressure

Stacking sequence	$\theta(°)$	2D Plate meshless RPIM (Liu et al, 2004) (15×15)	Present (2D FE Q4-SSM) (8×8)	Present (2D FE Q4-SSM) (10×10)
$[PZT/-\theta/\theta]_{as}$	15	7.222	7.235 (0.18%)	7.235 (0.18%)
$[PZT/-\theta/\theta]_{as}$	30	6.542	6.537 (−0.08%)	6.537 (−0.08%)
$[PZT/-\theta/\theta]_{as}$	45	6.217	6.221 (0.06%)	6.221 (0.06%)
$[PZT/-\theta/\theta]_s$	45	6.038	6.036 (−0.03%)	6.036 (−0.03%)

the non-dimensional transverse electric displacement $\tilde{D}_z = D_z/e_{31}$ displayed in Figs. 2.7 and 2.8 confirm that the IC constraints are satisfied.

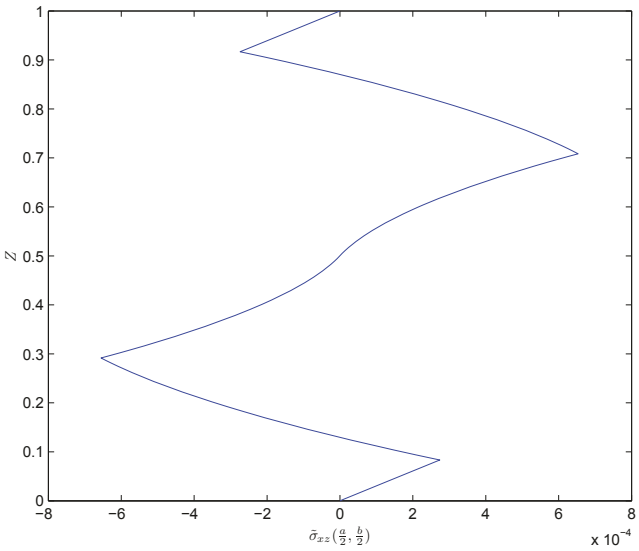

(a) Through-the-normalized ($Z = z/H$) thickness distribution of non-dimensional transverse shear stress $\tilde{\sigma}_{xz}$

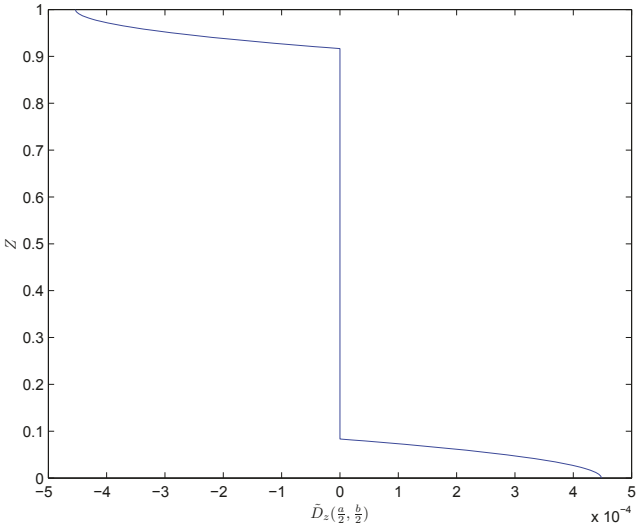

(b) Through-the-normalized ($Z = z/H$) thickness distribution of the non-dimensional transverse electric displacement $\tilde{D}_z$

Fig. 2.7. $[\mathrm{PZT}/-45°/45°]_{as}$ SS composite plate under uniform pressure

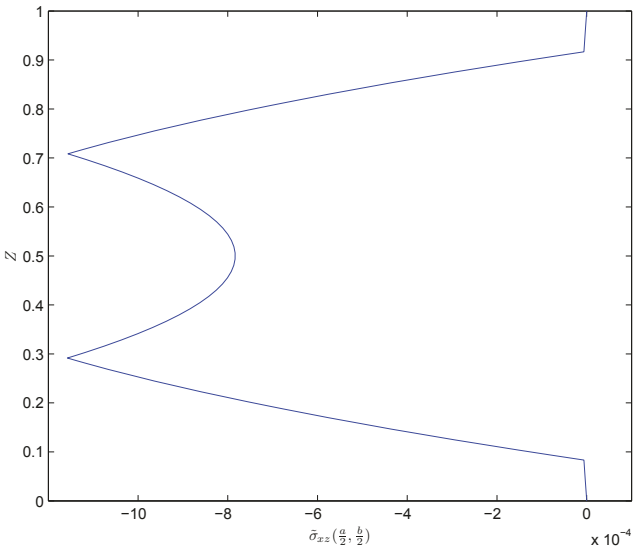

Fig. 2.8. Through-the-normalized thickness distribution of $\tilde{\sigma}_{xz}$ in the $[\mathrm{PZT}/-45^\circ/45^\circ]_s$ SS composite plate under uniform pressure

2.5 Conclusions and Perspectives

This chapter presented a new mixed Hamiltonian semi-analytical 3D static analysis solution. It is based on Lagrangian 2D in-plane FE discretization, allowing arbitrary edges BC, and mixed Hamiltonian VF, single-layer symplectic solution and propagator matrix through the thickness of the multilayer smart composite, allowing automatic satisfaction of the IC constraints. This combination of in-plane Lagrangian and through-the-thickness Hamiltonian formalisms, through the Legendre transformation, and the use of the nodal transverse stresses and electric displacement resultants as dual independent variables are the main originalities of the presented research work. It is applied to the analysis of multilayered piezoelectric structures static actuation and sensing and the comparison of the results with various reference solutions shows its rapid convergence and high accuracy. Moreover, the results also show that the present method is able to take into account realistic BC such as clamped and free edges, as well as non-classical multilayer composites stacking sequences such as symmetric and anti-symmetric angle-ply layups.

This work focused on presenting the detailed derivation of the new mixed Hamiltonian semi-analytic 3D solution with application to the static actuation and sensing of multilayered piezoelectric smart composites. It is worthwhile to investigate its extension to vibration and dynamic analyses.

References

Andrianarison O, Benjeddou A (2012) Hamiltonian partial mixed finite element-state space symplectic semi-analytical approach for the piezoelectric smart composites and FGM analysis. Acta Mechanica 223(8):1597–1610

Benedetti I, Aliabadi MH, Milazzo A (2010) A fast BEM for the analysis of damaged structures with bonded piezoelectric sensors. Computer Methods in Applied Mechanics and Engineering 199(9):490–501

Benjeddou A (2000) Advances in piezoelectric finite element modeling of adaptive structural elements: a survey. Computers & Structures 76(1–3):347–363

Benjeddou A, Andrianarison O (2005) A piezoelectric mixed variational theorem for smart multilayered composites. Mechanics of Advanced Materials and Structures 12(1):1–11

Benjeddou A, Deü JF (2001) Piezoelectric transverse shear actuation and sensing of plates, part 1: A three-dimensional mixed state space formulation. Journal of Intelligent Material Systems and Structures 12(7):435–449

Benjeddou A, Deü JF, Letombe S (2002) Free vibrations of simply-supported piezoelectric adaptive plates: an exact sandwich formulation. Thin-Walled Structures 40(7):573 – 593

Boffi D, Brezzi F, Fortin M (2013) Mixed Finite Element Approach and Applications. Springer, Berlin, Heidelberg

Carrera E, Büttner A, Nali P (2010) Mixed elements for the analysis of anisotropic multilayered piezoelectric plates. Journal of Intelligent Material Systems and Structures 21(7):701–717

Kapuria S, Kumari P, Nath JK (2010) Efficient modeling of smart piezoelectric composite laminates: a review. Acta Mechanica 214(1–2):31–48

Khandelwal RP, Chakrabarti A, Bhargava P (2013) An efficient hybrid plate model for accurate analysis of smart composite laminates. Journal of Intelligent Material Systems and Structures 24(16):1927–1950

Leung AYT, Zheng JJ, Lim CW, Zhang X, Xu XS, Gu Q (2008) A new symplectic approach for piezoelectric cantilever composite plates. Computers & Structures 86(19):1865–1874

Li D (2020) Layerwise theories of laminated composite structures and their applications: A review. Archives of Computational Methods in Engineering online first:1–24, DOI 10.1007/s11831-019-09392-2

Li S, Huang L, Jiang L, Qin R (2014) A bidirectional B-spline finite point method for the analysis of piezoelectric laminated composite plates and its application in material parameter identification. Composite Structures 107:346–362

Lim CW, Xu XS (2010) Symplectic Elasticity: Theory and Applications. Applied Mechanics Reviews 63(5):1–10

Liu GR, Dai KY, Lim KM (2004) Static and vibration control of composite laminates integrated with piezoelectric sensors and actuators using the radial point interpolation method. Smart Materials and Structures 13(6):1438–1447

Moleiro F, Mota Soares CM, Mota Soares CA, Reddy J (2015) Layerwise mixed models for analysis of multilayered piezoelectric composite plates using least-squares formulation. Composite Structures 119:134 – 149

Pablo F, Bruant I, Polit O (2009) Use of classical plate finite elements for the analysis of electroactive composite plates. Numerical validations. Journal of Intelligent Material Systems and Structures 20(15):1861–1873

Phung-Van P, Lorenzis LD, Thai CH, Abdel-Wahab M, Nguyen-Xuan H (2015) Analysis of laminated composite plates integrated with piezoelectric sensors and actuators using higher-order shear deformation theory and isogeometric finite elements. Computational Materials Science 96(PartB):495 – 505

Shan L, Jun L, Gao L, Zhang Z, Zhang P (2018) The static solution for the layered piezoelectric bounded domain with side face load by the modified SBFEM. Advances in Applied Mathematics and Mechanics 10:209–241

Sze KY, Pan YS (1999) Hybrid finite element models for piezoelectric materials. Journal of Sound and Vibration 226(3):519 – 547

Tahani M, Naserian-Nik AM (2013) Bending analysis of piezolaminated rectangular plates under electromechanical loadings using multi-term extended Kantorovich method. Mechanics of Advanced Materials and Structures 20(6):415–433

Tzou HS (1989) Development of a light-weight robot end-effector using polymeric piezoelectric bimorph. In: Proceedings, 1989 International Conference on Robotics and Automation, IEEE, Scottsdale, AZ, vol 3, pp 1704–1709

Tzou HS (1993) Piezoelectric Shells: Distributed Sensing and Control of Continua. Kluwer Academic Publishers

Vidal P, D'Ottavio M, Thaïer MB, Polit O (2011) An efficient finite shell element for the static response of piezoelectric laminates. Journal of Intelligent Material Systems and Structures 22(7):671–690

Wu CP, Liu YC (2016) A review of semi-analytical numerical methods for laminated composite and multilayered functionally graded elastic/piezoelectric plates and shells. Composite Structures 147:1–15

Zhang WX, Wang H (2018) Axisymmetric boundary condition problems for transversely isotropic piezoelectric materials. Mechanics Research Communications 87:7 – 12

Zhou Y, Li S, Zhou H (2015) State space finite element analysis for piezoelectric precision positioning considering secondary converse piezoelectric effect. Finite Elements in Analysis and Design 102-103:85 – 94

Zhou Y, Nyberg T, Xiong G, Li S (2020) State space finite element analysis for piezoelectric laminated curved beam with variable curvature. Mechanics of Advanced Materials and Structures 27(4):265–273